17th Australasian Fluid Mechanics Conference
Auckland, New Zealand
5-9 December 2010

Conditional large-scale structure of a high Reynolds number turbulent boundary layer

N. Hutchins[1], J. P. Monty[1], B. Ganapathisubramani[2], H. Ng[1] & I. Marusic[1]

[1]Department of Mechanical Engineering
The University of Melbourne, Victoria, 3010 AUSTRALIA

[2]Department of Aeronautics, Imperial College London,
Prince Consort Road, London, SW7 2AZ, UK

Abstract

A spanwise array of 10 surface mounted hot-film shear-stress sensors coupled with a traversing hot-wire probe are used to identify the conditional structure associated with a large-scale skin-friction event in a high Reynolds number turbulent boundary layer ($Re_\tau \approx 14000$). Instantaneous shear-stress data indicate the presence of large-scale structures at the wall that are comparable in scale and arrangement to the superstructure events as reported previously by Refs (4; 5). Conditional averages of streamwise velocity computed based on a low skin-friction footprint at the wall offer a wider three-dimensional view of the average superstructure event. These events consist of highly elongated forward-leaning low-speed structures, flanked on either side by high speed events of similar general form. An analysis of small-scale energy associated with these large-scale events reveals that the small-scale velocity fluctuations are modulated by the presence of large-scale features. In general it is observed that the attenuation and amplification of the small-scale energy seems to approximately align with large-scale regions of streamwise acceleration and deceleration respectively. These results suggest that small-scale structures, including near-wall streaks/vortices, are influenced by the passage of outer layer large-scale events. Therefore, any control strategy for high Reynolds number wall-bounded turbulence that aims to control the small-scale activity in the near-wall region will likely need to account for the behaviour of the large-scale structures that are present in the outer layer. The results might also suggest the viability of specifically targeting the large-scale structure in order to control turbulence.

Facility & Measurement Array

Experiments are performed in the High Reynolds Number Boundary Layer Wind-Tunnel (HRNBLWT) at the University of Melbourne, an open-return blower wind-tunnel with a working section, $2 \times 1 \times 27$ m. Full details of the facility are available in ref (10). Measurements were performed in the turbulent boundary layer developing over the tunnel floor approximately 21 m downstream of the tripped inlet to the working section. Freestream velocity (U_∞) was 20.33 ms^{-1} (and freestream turbulence intensity $\sqrt{\overline{u_\infty^2}}/U_\infty = 0.2\%$). The boundary layer thickness (δ) at the measurement location was 0.326 m yielding a Kárman number, $Re_\tau = \delta U_\tau/\nu = 14200$ (where, ν is the kinematic viscosity and U_τ is friction veloicty). Throughout this paper, *x*, *y* and *z* will be used to denote the streamwise, spanwise and wall-normal axes, with *u*, *v* and *w* denoting the respective fluctuating velocity components. Capitalised velocities (e.g. U) or overbars (e.g. $\overline{u} = 0$) indicate time-averaged values. Angle brackets (e.g $\langle u \rangle$) denote conditionally averaged quantities. The superscript $^+$ is used to denote viscous scaling of length (e.g. $z^+ = zU_\tau/\nu$), velocity ($U^+ = U/U_\tau$) and time ($t^+ = tU_\tau^2/\nu$).

A spanwise array of 10 flush-mounted hot-film sensors are affixed to the tunnel wall 21m downstream of the inlet to the working section. This array covers a spanwise domain of $\sim 0.7\delta$, with a spanwise resolution $\Delta y_{\rm hf} = 0.026$ m or 0.08δ. The 10 Dantec 55R47 glue-on flush-mounted sensors are operated in constant temperature mode using *AA labs AN1003* anemometers with overheat ratio (OHR) set to approximately 1.05. The active spanwise length of the sensor $l_{\rm hf}$ (0.9 mm) equates to a viscous-scaled length $l_{\rm hf}^+ = 39$ for this experiment. The sensors are numbered sequentially from 1 to 10 as indicated in figure 1.

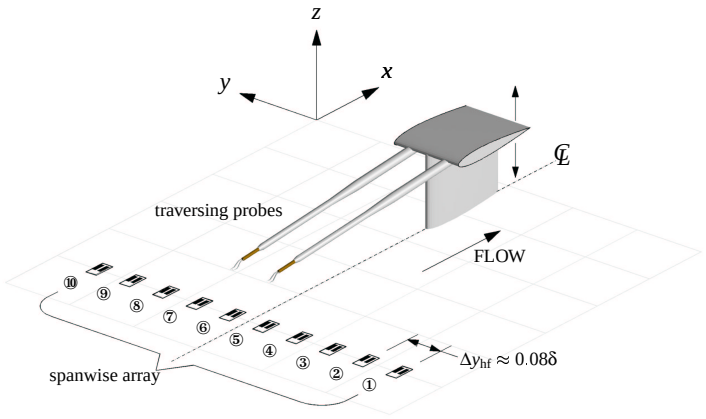

Figure 1: Diagram detailing the measurement array.

Two hot-wire probes are mounted above the spanwise array in a wall-normal traverse. Two sensors were employed to minimise inaccuracy due to calibration drift, but for this report only the data from the left hand-side sensor in figure 1 is analysed (this probe is located almost exactly above hot-film sensor 6). This hot-wire probe has an etched sensor length of $l = 0.5$ mm (equating to $l_{\rm hw}^+ \approx 22$ for the current experimental conditions). The suffixes 'hf' and 'hw' will be used to denote the hot-film and hot-wire sensors, respectively.

Instantaneous fluctuations from the spanwise array

Hot-film sensors are known to suffer from reduced frequency response (as compared to hot-wires) due to heat conduction to the substrate (see 3). A careful comparison between the hot-film measured spectra and that measured by hot-wire sensors located very close to the wall, reveals that for frequency content $> 50Hz$ there is an increasing attenuation of the hot-film measured statistics. Assuming a constant convection velocity (discussed below), this equates to attenuation of streamwise length-scales $< 0.5\delta$. In light of this analysis, the signals from the hot-film sensors are filtered using a 2-D gaussian (with approximate length 0.5δ and spanwise width 0.16δ) to leave only the large-scale component of the signal. As a precursor to these experi-

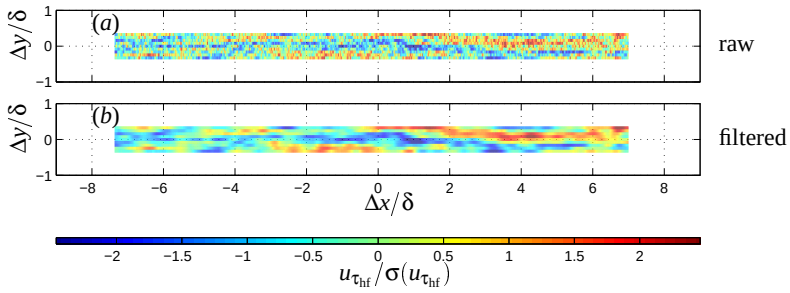

Figure 2: Example velocity signals from the spanwise array (*a*) unfiltered raw data; (*b*) 2-D Gaussian filter of size $0.5\delta \times 0.16\delta$ (streamwise, spanwise) applied. Colour shows fluctuating skin friction velocity normalised by the standard deviation. Signals are projected in *x* using Taylors Hypothesis and a convection velocity of $U_c^+ = 20$.

ments, the spanwise array of 10 sensors was also rotated by 90° to produce a streamwise array. Cross-correlation of the large-scale component of *u* fluctuations measured by this streamwise array enable a determination of the convection velocity of the large-scale structure at the wall. It was found that the large-scale events have a convection velocity $U_c \approx 13.3ms^{-1}$ (equating to $U_c^+ \approx 20$). This convection velocity has been employed throughout the subsequent analysis.

Figure 2(*a*) shows a short period of the fluctuating skin friction signals from the spanwise array projected spatially using Taylor's hypothesis and the measured large-scale convection velocity. It is immediately evident from this plot that highly elongated meandering low- and high shear-stress regions are present in the skin friction field at the wall. The scale and form of these fluctuations is strikingly similar to the 'superstructure'-type events observed in the log region of high Reynolds number turbulent boundary layers by (5). Figure 2(*b*) shows the same snippet of data with the Gaussian filter applied. This filter removes the unreliable high frequency ($> 50Hz$) hot-film fluctuations that are beyond the attenuation limit of the hot-film sensors. Figure 2(*b*) shows that despite the limited frequency response, the hot-film array has sufficient dynamic range to capture the largest-scale skin friction events (which are the focus of this study). Throughout the proceeding analysis, the hot-films are only used as a 'detector' probe for the large-scale events, the precise value of the standard deviation and any attenuation of small-scales will be of little impact to the analysis, since they are only used to detect the passage of low or high skin friction events.

Conditional analysis

The relationship between the skin-friction fluctuations and the velocity fluctuations can be examined by computing conditional quantities from the hot-wire probe conditioned on the presence of a low/high skin-friction event. A low skin-friction event occurs when the instantaneous skin friction fluctuation is less than zero ($\tau_w < 0$) and conversely a high skin-friction event occurs when the fluctuation is greater than zero ($\tau_w > 0$, where τ_w is the Gaussian filtered fluctuating wall shear stress). Note that no thresholds are used anywhere in this analysis; events are discriminated only on sign. Figure 3(*a*) & (*b*) show the conditional mean velocity and turbulence intensity profiles computed using the traversing hot-wire and just the hot-film sensor that is located directly below the traversing sensor (hf6). The unconditional profiles are plotted (○) together with the conditional quantities for large-scale low (▽) and high (△) skin-friction events. The velocity statistics are scaled with the unconditional mean friction velocity, U_τ. It is immediately clear from figure 3*a* that a low skin-friction event is associated with a velocity profile that

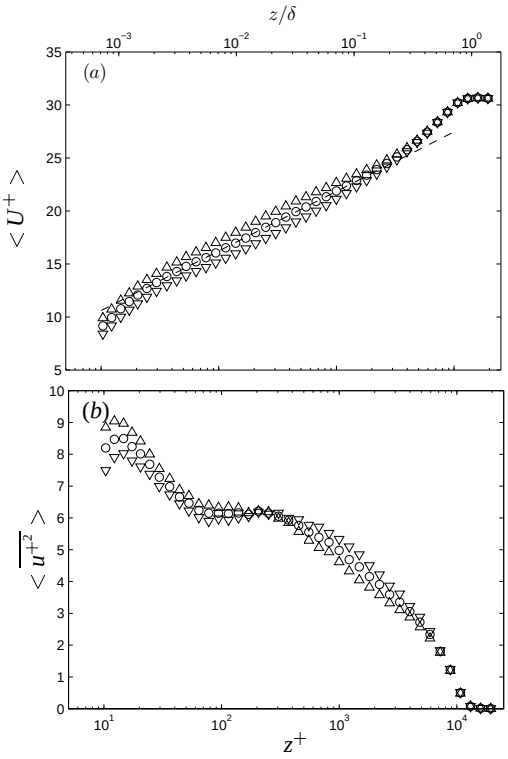

Figure 3: Mean (*a*) velocity and (*b*) turbulence intensity profiles conditionally-averaged on (▽) low and (△) high shear stress events; (○) show unconditional profiles.

is consistently lower than the unconditional mean throughout the near-wall and logarithmic regions. Similarly, a high skin-friction event has a velocity profile that is consistently higher than the mean. Figure 3(*b*) demonstrates that a large-scale low-shear stress event has attenuated turbulence intensity close to the wall, switching to amplified turbulence intensity in the log region. The opposite is true for the large-scale high skin friction event. Spectral decomposition demonstrates that this modulation occurs primarily within the small-scales.

The results shown above are with zero time shift (i.e they represent the conditional profile observed by the hot wire sensor at the same instant that hf6 detects eithers a low or high skin friction event. The simultaneous acquisition of skin-friction and hot-wire time-series also allow us to compute conditionally-averaged velocity profiles that occur prior to or after a low or high skin-friction event. Moreover, although the hot-wire probe

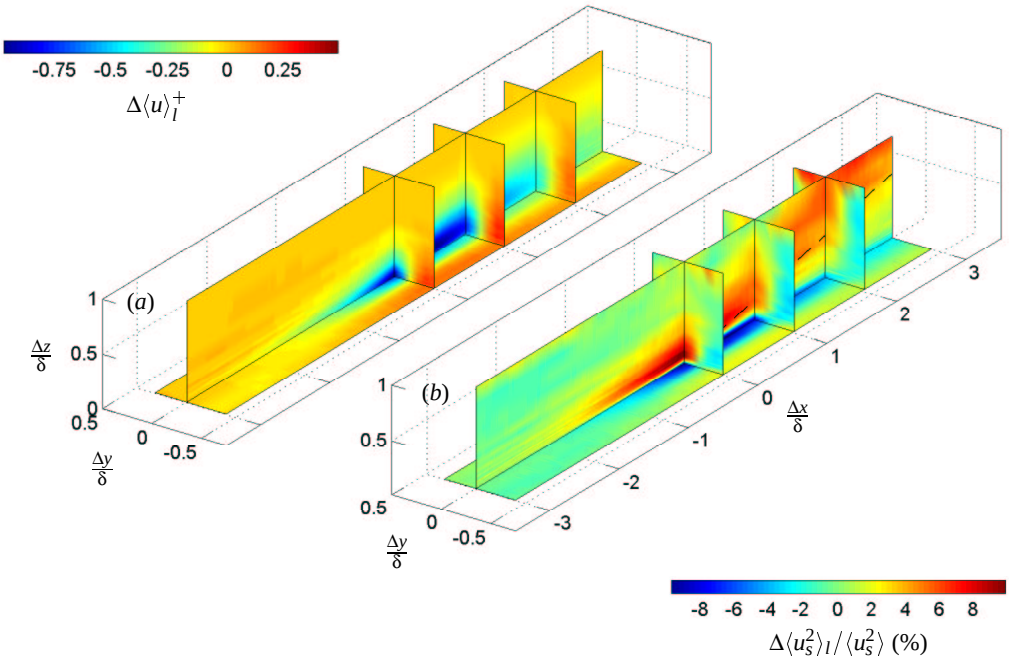

Figure 4: Iso-contours of (*a*) streamwise velocity conditionally averaged on a low shear stress event. (*b*) streamwise small-scale variance conditioned on a low shear stress event. Variance data are presented as a percentage fluctuation about the unconditioned small-scale variance.

is located above hot-film 6, the remaining hotfilm sensors (hotfilms 1–5 and 7–10) can be used to determine the conditional hotwire signal at some spanwise shift $N\Delta y_{\rm hf}$, where N is an integer (between -5 and 4) and $\Delta y_{\rm hf}$ is the spanwise spacing between hotfilms in the array. This process enables us to construct a full three-dimensional view of the conditional event associated with a negative or positive large-scale skin friction fluctuation at the wall. Since negative skin friction conditional averages are, for the purposes of this investigation, simply the inverse of the high-speed conditional averages, we will consider only one of these cases (negative) for the remainder of this study. The conditional average of mean fluctuations based on a low skin friction event is defined as,

$$\langle u\rangle_l(\Delta t,\Delta y,z) = \langle u(t,y,z) \;\mid\; u_\tau(t-\Delta t, y-\Delta y) < 0\rangle \qquad (1)$$

Or converting Δt to Δx using Taylor's hypothesis,

$$\langle u\rangle_l(\Delta x,\Delta y,z) = \langle u(x,y,z) \;\mid\; u_\tau(x-\Delta x, y-\Delta y) < 0\rangle \qquad (2)$$

Figure 4(*a*) shows iso-contours of $\Delta\langle u\rangle_l^+$ in various $x-y$, $y-z$ and $x-z$ planes, offering a three-dimensional view of the conitioned mean velocity signature associated with a low skin friction event. The $x-z$ plane is extracted along $\Delta y = 0$ and the $x-y$ plane shown is located at $z/\delta = 7\times10^{-4}$ (the closest position to the wall from the hot-wire traverse). This figure reveals a highly inclined, forward-leaning, low speed structure extending beyond 3δ in the downstream direction and 2δ upstream. In the spanwise direction ($y-z$ planes), there is a clear high-low-high conditional velocity behaviour also documented previously through two-point correlations. The features of this structure are generally consistent with various other correlation studies in the literature (2; 8, among others), and also consistent with the recent emergent view of very large-scale motions (7) or superstructure events (5). The width of the low speed region appears to be approximately 0.5δ at $\Delta x = 0$. Although the spanwise and wall-normal components of the velocities are not measured in this study, results from DNS data (6) suggest that the observed adjacent low- and high-speed regions are associated with a pair of counter-rotating roll modes.

Refs. (1), (6) and (9) have shown that large-scale structures in turbulent boundary layers can modulate the amplitude of the small scale energy. Here we investigate this phenomenon by producing a conditional average of the small-scale fluctuations from the hot-wire signal, based upon the occurrence of a large-scale low skin friction event at the wall. The first step in this analysis is to decompose the hotwire signal (hw2) into a small-scale component using a sharp spectral cut-off filter at $\lambda_x^+ = 7300$ (where λ_x is the streamwise wavelength). This filtered small-scale signal is called u_s. The conditional analysis is then very similar to that described in equations (1) and (2), We use the same condition event (the occurrence of a large-scale negative skin friction event), only in this case we ensemble average the small-scale variance (see equation 3).

$$\langle u_s^2\rangle_l(\Delta x,\Delta y,z) = \left\langle u_s^2(x,y,z) \;\mid\; u_\tau(x-\Delta x, y-\Delta y) < 0\right\rangle \qquad (3)$$

Figure 4(*b*) presents three-dimensional views of the conditioned small-scale variance. The colour scale shows percentage change in small-scale variance, $(\langle u_s^2\rangle_l/\overline{u_s^2} - 1)\times 100$. Red shading shows increased small-scale energy, and blue shows reductions. With zero timeshift, Mathis *et al.* (9) have shown that within a large-scale negative u fluctuation the small-scale energy is attenuated close to the wall, but that this behaviour switches at $z \approx \sqrt{15Re_\tau}$, above which point the small-scale energy is increased. Such behaviour is clearly evident in the conditional variance plots of figure 4(*b*). At $\Delta x = 0$, the reduced small-scale energy (blue contours) changes to increased small-scale energy (red contours) around $z^+ \approx 450$ ($z \approx 0.32\delta$, very close to $\sqrt{15Re_\tau}$ for the current Reynolds number). However, the wider three-dimensional view afforded by figure 4(*b*) shows that the crossover between reduced and increased small-scale energy is actually inclined in x. The dashed line on figure 4(*b*) shows the streamwise minima of the conditioned velocity fluctuations (as shown in figure 4*a*). This line is observed to very closely trace the separation between increased and reduced small-scale activity (the separation between red and blue contours on figure 4*b*). The streamwise minima of the conditioned velocity fluctuations is significant in that it demarcates a region of deceleration

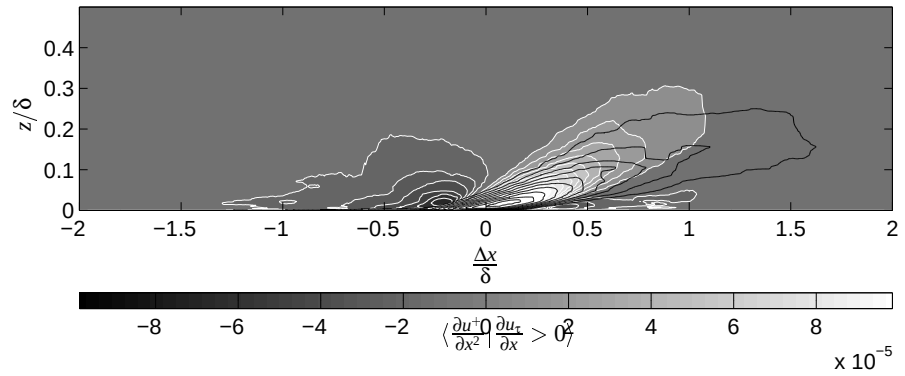

Figure 5: A large scale event conditioned on the occurrence of positive $\frac{\partial u_\tau}{\partial x}$ at the wall. Filled gray-shaded contours (with white outline) show $\langle \frac{\partial u}{\partial x} | \frac{\partial u_\tau}{\partial x} > 0 \rangle$ (white is positive $\frac{\partial u}{\partial x}$ and darkest gray is negative $\frac{\partial u}{\partial x}$, see colour scale below figure). The solid black contours show regions in which the small-scale turbulence intensity is attenuated. Contours show $\Delta\langle u_s^2 | \partial_x u_\tau > 0 \rangle / \overline{u_s^2}$ from -10% to -1% in increments of 1%.

($-du/dx$ upstream of the dashed line) from a region of acceleration ($+du/dx$ downstream of the dashed line). In short, figure 4 seems to imply that increased small-scale activity might be associated with locally streamwise decelerating large-scale flows, and conversely attenuated small-scale activity is associated with locally accelerating large-scale flows. To test this hypothesis, a conditional analysis was performed based on the occurrence of a positive streamwise skin friction gradient.

Figure 5 shows the conditionally averaged velocity gradient based on positive $\frac{\partial u_\tau}{\partial x}$ for the streamiwse/wall-normal plane at $\Delta y = 0$. The shaded contours show the conditional velocity gradient as calculated from,

$$\left\langle \frac{\partial u}{\partial x} \right\rangle_{+\text{ve}} (\Delta x, \Delta y, z) = \left\langle \frac{\partial u}{\partial x} \;\middle|\; \frac{\partial u_\tau}{\partial x}(x + \Delta x, \Delta y) > 0 \right\rangle. \quad (4)$$

A relatively compact negative-postive-negative behaviour of the contours in the streamwise direction is exhibited. The importance of the region of strong positive streamwise velocity gradient is highlighted by its coincidence with the region of attenuation of the small-scale velocity fluctuations. The conditionally averaged small-scale variance is calculated on the occurrence of a positive skin friction gradient. This is plotted as solid line contours in figure 5 which show percentage change in the small-scale variance ($\langle u_s^2 \rangle_{+ve} / \overline{u_s^2} - 1$). The contours are plotted on top of shaded contours of the conditional velocity gradient event. The similarities between both sets of contours shown in figure 5 is striking. The streamwise gradient and small-scale variance conditional averages are both similarly inclined, albeit at slightly different angles. They occupy similar spatial regions and most notably the maximum velocity gradient occurs very close to the maximally attenuated small-scale variance. In short, the modulation of small-scale energy within the turbulent boundary layer appears to be strongly associated with the large-scale streamwise velocity gradients brought about by the superstructure events. That is, the superstructure events produce large-scale regions of streamwise acceleration and deceleration, which respectively correspond to attenuation and amplification of small-scale events.

Conclusions

The close spacing ($\lesssim 0.25\delta$) of the negative and positive velocity gradient peaks in figure 5 and general compactness of the contours is somewhat surprising. There appears no obvious reason from the conditional event $\langle u \rangle_I$ shown in figure 4 for such sharp transitions (spatially) from strong negative gradient to strong positive around the superstructure event. The tentative suggestion at this stage is that a spanwise meandering of the largest scale structures (as observed by (5)) can lead to aggressive streamwise gradients, that in turn appear to be associated with amplification of small-scale turbulence.

References

[1] Bandyopadhyay, P. R. and Hussain, A. K. M. F., The coupling between scales in shear flows, *Phys. Fluids*, **27(9)**, 1984, 2221–2228.

[2] Brown, G. R. and Thomas, A. S. W., Large structure in a turbulent boundary layer, *Phys. Fluids*, **20**, 1977, S243–S251.

[3] Bruun, H. H., *Hot-wire anemometry*, Oxford University Press, 1995.

[4] Ganapathisubramani, B., Clemens, N. T. and Dolling, D. S., Effects of upstream boundary layer on the unsteadiness of shock induced separation, *J. Fluid Mech.*, **585**, 2007, 369–394.

[5] Hutchins, N. and Marusic, I., Evidence of very long meandering structures in the logarithmic region of turbulent boundary layers, *J. Fluid Mech.*, **579**, 2007, 1–28.

[6] Hutchins, N. and Marusic, I., Large-scale influences in near-wall turbulence, *Phil. Trans. R. Soc. Lond.*, **365**, 2007, 647–664.

[7] Kim, K. C. and Adrian, R. J., Very large-scale motion in the outer layer, *Phys. Fluids*, **11**(2), 1999, 417–422.

[8] Kovasznay, L. S. G., Kibens, V. and Blackwelder, R. F., Large-scale motion in the intermittent region of a turbulent boundary layer, *J. Fluid Mech.*, **41**, 1970, 283–326.

[9] Mathis, R., Hutchins, N. and Marusic, I., Large-scale amplitude modulation of the small-scale structures in turbulent boundary layers, *J. Fluid Mech.*, **628**, 2009, 311–337.

[10] Nickels, T. B., Marusic, I., Hafez, S. and Chong, M. S., Evidence of the k^{-1} law in high-reynolds number turbulent boundary layer, *Phys. Rev. Lett.*, **95**, 2005, 074501.